Materials Characterization 216 (2024) 114249

Contents lists available at ScienceDirect

Materials Characterization

journal homepage: www.elsevier.com/locate/matchar

Microstructure of shell and grain boundary phase in Nd-Fe-B sintered magnets grain boundary diffusion processed with low-melting LRE-Al-Cu (LRE = La and Pr) alloys

Ye Ryeong Jang [a], Tae-Hoon Kim [b], Jeongmin Kim [c], Hyun-sook Lee [a], Kyungmi Lee [a], Jong Wook Roh [d], Tae-Suk Jang [e], Wooyoung Lee [a,*]

[a] Department of Materials Science and Engineering, Yonsei University, Seoul 03722, Republic of Korea
[b] Department of Magnetic Materials, Korea Institute of Materials Science, Changwon 51508, Republic of Korea
[c] Division of Nanotechnology, Daegu Gyeongbuk Institute of Science & Technology, Daegu, 42988, Republic of Korea
[d] School of Nano & Materials Science and Engineering, Kyungpook National University, Gyeongsangbuk-do 37224, Republic of Korea
[e] Department of Advanced Materials Engineering, Sunmoon University, Asan, 336-708, South Korea

ARTICLE INFO

Keywords:
Nd-Fe-B
Grain boundary diffusion
Light rare-earth
LRE-Al-Cu
Chemically induced liquid film migration

ABSTRACT

We report magnetic and microstructural changes in Nd-Fe-B sintered magnets after the grain boundary diffusion process (GBDP) of low-melting LRE-Al-Cu alloys [LRE (Light Rare-earth) = La and Pr]. A distinctive microstructural feature of the magnets GBD treated with La-Al-Cu (LAC) and Pr-Al-Cu (PAC) were characterized *via* the electron probe microanalysis and high-angle annular dark-field scanning transmission electron microscopy analysis at a depth of 50 μm from the magnet surface. The formation of a thick high-anisotropy Pr-Al-rich shell was clearly observed in the PAC-GBDP magnets, whereas there was no distinct shell formation in the LAC-GBDP magnets. La, Al, and Cu were dissolved in the Nd-rich grain boundary phase (GBP) rather than in the main phase, thereby thickening the GBP. This resulted in a difference in the coercivity gain between PAC-GBDP (+6.4 kOe) and LAC-GBDP (+3.3 kOe). The point to note here is that the remanence reduction induced by LAC-GBDP (−0.2 kG) is much smaller than that induced by PAC-GBDP (−1.2 kG) because the grain boundary diffused La-Al-Cu, which can dilute the saturation magnetization of the $Nd_2Fe_{14}B$ (2–14-1) crystal, does not dissolve into 2–14-1. Furthermore, the squareness of demagnetization curves of the LAC-GBDP magnets (98%) was much improved than that of the PAC-GBDP magnets (86%). This is because chemically induced liquid film migration (CILFM), an undesirable grain growth phenomenon induced by shell formation, does not occur in LAC-GBDP magnets. In conclusion, the deterioration in remanence and squareness, which are serious problems in the LRE-GBDP, can be minimized by the LAC-GBDP; thus, the utilization of La in the GBDP is a promising method for obtaining a high maximum energy product of the magnets. Based on the results of this analytical work, we propose a guide for developing a cost-effective novel GBDP source that can prevent grain growth by CILFM and increase the magnetocrystalline anisotropy of the shell.

1. Introduction

Nd-Fe-B sintered magnets have an excellent maximum energy product; however, their thermal stability in terms of coercivity (H_{cj}) is relatively poor. Therefore, to apply them to motors operating at temperatures above 150 °C, such as traction motors in electric vehicles, H_{cj} at room temperature needs to be sufficiently increased [1–4]. Replacing the Nd in $Nd_2Fe_{14}B$ (2:14:1) with heavy rare-earth (HRE) elements, such as Tb and Dy, is one of the efficient ways to enhance the H_{cj} of the magnets because the anisotropy field of the 2:14:1 phase increases as its HRE concentration increases; however, this causes the degradation in remanence (B_r) and maximum energy product [$(BH)_{max}$] of the magnets due to the antiferromagnetic coupling between the HRE and Fe atoms in the 2:14:1 [5,6]. In addition, owing to the shortage of HRE resources, there is a strong demand for enhancing the H_{cj} of magnets with minimal use of HRE [7]. To overcome these limitations, a Grain Boundary Diffusion Process (GBDP) developed in 2005 by Hirota *et al* [8]. GBDP facilitates the diffusion of HRE along the grain boundary phase (GBP),

* Corresponding author.
E-mail address: wooyoung@yonsei.ac.kr (W. Lee).

https://doi.org/10.1016/j.matchar.2024.114249
Received 13 June 2024; Received in revised form 20 July 2024; Accepted 6 August 2024
Available online 8 August 2024

thereby forming a high-anisotropy HRE-rich shell only on the 2:14:1 grain surface, where the reverse domain is likely to nucleate [9–11]. As a result, the H_{cj} of the magnets was significantly improved without B_r reduction, even when a small amount of HRE was used. However, the supply risk of HRE in manufacturing high-H_{cj} magnets is still a major concern; thus, research interest in developing HRE-free GBDP has recently increased [7,12–15].

Akiya *et al* first introduced the use of LRE-based Nd/Pr-Cu eutectic alloys in the development of the HRE-free GBDP of sintered and hot-deformed Nd-Fe-B bulk magnets [16]. Unlike HRE-GBDP, the H_{cj} enhancement of magnets subjected to LRE-GBDP is mainly attributed to the modification of the morphology and chemistry of the Nd-rich GBP [17]. Homogeneous and continuous non-ferromagnetic GBP enriched with RE and Cu, which can effectively weaken the exchange interactions between hard magnetic grains, are formed after the Nd/Pr-Cu GBDP [16]. In addition, the diffusion of a low-melting-point eutectic alloy with good wettability can smoothen and flatten the GBP//2:14:1 interface, thereby reducing the defect density on the grain surface and suppressing the nucleation of the reverse domain [17]. However, in this case, the B_r of the magnets [$B_r = f(1\text{-}V_{non\text{-}ferro})M_s$, f: [001]-texture, $V_{non\text{-}ferro}$: volume fraction of non-ferromagnetic phases] decreases substantially owing to a dramatic increase in the volume fraction of non-ferromagnetic GBP ($V_{non\text{-}ferro}$) in the magnets after GBDP [18]. To further improve the H_{cj} and B_r of LRE-GBDP magnets, various LRE-containing sources, such as La–Al–Cu [19–21], Nd—Cu [22–24], Pr—Cu [25], Pr–Al–Cu [19,26] and Pr-Nd-Al [27] have been used as sources for GBDP. Among the LRE-containing alloys for the GBDP, the Pr-containing alloys showed different effects on the microstructure and H_{cj} of the magnets after the GBDP. The Pr-containing alloy GBDP (Pr-GBDP) not only modifies the microstructure of Nd-rich GBP but also forms a high-anisotropy Pr-rich shell in magnets [28–31]. As a result, H_{cj} obtained by Pr-GBDP is much higher than that obtained by Nd-GBDP or La-GBDP. However, owing to Pr-rich shell formation, undesirable grain growth occurs in magnets after Pr-GBDP because chemically induced liquid film migration (CILFM) occurs during Pr-rich shell formation, as reported by Kim *et al* [32]. Therefore, the H_{cj} improvement is limited, and the squareness of the magnets decreases after Pr-GBDP [33,34]. According to previous investigation [19–21,35–37], low-melting alloys designed based on La, a highly cost-effective rare-earth element, seem to be a prospective source for inhibiting CILFM during GBDP because the grain boundary diffused La does not contribute to shell formation [19–21,35–37]. La is segregated into GBP only because $La_2Fe_{14}B$ is much more unstable than $Nd_2Fe_{14}B$. Consequently, a very thick Nd-rich GBP containing a large amount of paramagnetic La was formed after the La-GBDP [19–21,35–37]. However, the H_{cj} gain by La-GBDP is only about 2.2 kOe, and the origin of the low-H_{cj} of La-GBDP magnets remains unclear [19–21]. Thus, although La appears to be an effective GBDP source for inhibiting CILFM, as reported by Zhao et al. [35], its utilization has been limited.

The magnetic and microstructural changes caused by LRE-GBDP largely depend on the type of source of the GBDP, as described above. However, the microstructural features of LRE-GBDP magnets have not been clearly reported. In order to get a clue to further modify the microstructure and H_{cj} of the LRE-GBDP magnets, their microstructure should be intensively characterized, specifically focusing on the microstructure of shell and RE-rich GBP that are the critical determinants of the H_{cj} of magnets. Herein, we comparatively investigated the magnetic and microstructural properties of Nd–Fe–B magnetic GBD treated with La–Al-Cu and Pr-Al-Cu. The distinct effects of La-GBDP and Pr-GBDP on the shell formation and microstructure of Nd-rich GBP were clarified, and the origin of their microstructural characteristics was elucidated in terms of the CILFM phenomenon. Based on our findings, a guide for obtaining higher H_{cj} and B_r in magnets using cost-effective LRE-GBDP was proposed.

2. Experimental

A commercial 48 M graded (Nd, Pr)–Fe–B sintered magnet (12.5 mm × 12.5 mm × 5 mm, Advanced Technology & Materials Co., Ltd.) was selected as a base magnet. The surface of the as-sintered magnet was etched using a 2% nitric acid solution for 20s to remove any oxide layers on the magnet surface. Low-melting-point ternary $LRE_{70}Al_{20}Cu_{10}$ (LRE = La and Pr) ribbon alloy compounds fabricated by melt-spinning were used as grain boundary diffusion sources. Alloy ribbons with a thickness of ~60 μm, which were cut to fit the size of the magnet, were attached to the top and bottom surfaces perpendicular to the alignment direction (c-axis) of the as-sintered magnet using polyvinyl alcohol (PVA). The average mass of the ribbon used for coating was adjusted to approximately 2.1 wt% of the magnet. In order to determine the optimal grain boundary diffusion temperature, the magnets covered with the alloy ribbons were heat-treated at various temperatures within the range of 750 to 900 °C for 1 h in a vacuum. The magnets were then annealed at 500 °C for 3 h under an Ar atmosphere. To determine effect of heat treatment on magnetic properties, as-sintered magnet was also heat treated at 800 °C for 1 h followed by an annealing at 500 °C for 3 h without application of diffusion sources, which was named annealed magnet. The thermal behavior of the diffusion sources was analyzed using differential scanning calorimetry (DSC), and the demagnetization curves of the as-prepared magnets were measured at room temperature using a B—H hysteresis loop tracer (Permagraph C-300, Magnet-Physik). The microstructure of the magnets and the distribution of diffused elements in the magnets were analyzed using field-emission electron probe microanalysis (FE-EPMA; JXA 8530F, JEOL) and field-emission scanning transmission electron microscopy (FE-STEM; Talos F200X, Thermo Fisher Scientific), respectively.

3. Results and discussion

Fig. 1(a)–(c) show the changes in the coercivity (H_{cj}), remanence (B_r), and maximum energy product [$(BH)_{max}$] of the GBD treated Nd-Fe-B magnets as a function of the GBD temperature. For comparison, the magnetic properties of the as-sintered and annealed base magnets are indicated by black and gray dotted lines, respectively. The optimum GBDP temperature, which can obtain the highest H_{cj} value, was 800 °C for the $La_{70}Al_{20}Cu_{10}$ (LAC)- and $Pr_{70}Al_{20}Cu_{10}$ (PAC)-GBDP as shown in the red and green circles of Fig. 1(a). The H_{cj} gain after the LAC- and PAC-GBDP at their optimum temperatures were 6.4 and 3.3 kOe, respectively, which indicates that the PAC is more effective source for enhancing the H_{cj} of magnets compared to the LAC. However, the H_{cj} improvement by PAC-GBDP is accompanied by a dramatic decrease in B_r and $(BH)_{max}$, as shown in Fig. 1(b) and (c). According to a previous investigation of Pr-GBDP, the volume fraction of nonferromagnetic GBP enriched with Pr or Nd substantially increases after GBDP, thereby improving H_{cj} while deteriorating the B_r and $(BH)_{max}$ of the magnets [19,26,27]. Therefore, the magnetic property changes caused by the PAC-GBDP shown in Fig. 1(a)–(c) are a common and predictable result. Notably, H_{cj} enhancement with only a slight B_r reduction was achieved using LAC-GBDP. Considering the influence of La on the intrinsic magnetic properties of 2–14-1 [38], it is expected that both H_{cj} and B_r of the Nd-Fe-B magnets would decrease after LAC-GBDP if La diffused into 2–14-1 and was substituted with Nd; however, as shown in Fig. 1 (a)–(c), H_{cj} increases by 3.3 kOe and the B_r decreases by only 0.2 kG after the LAC-GBDP. This indicates that the LAC source exhibits a distinct diffusion behavior that does not affect the intrinsic magnetic properties of the 2–14-1 main phase in the magnets. Furthermore, as shown in Fig. 1(d) and Table 1, the squareness of the demagnetization curve of the LAC-GBDP magnets (98%) was significantly better than that of the PAC-GBDP magnets (86%). According to recent investigations, the squareness of the magnets deteriorates after GBDP when the uniformity of the grain size becomes poor owing to grain growth by chemically induced liquid film migration (CILFM) occurring during shell formation [32–34].

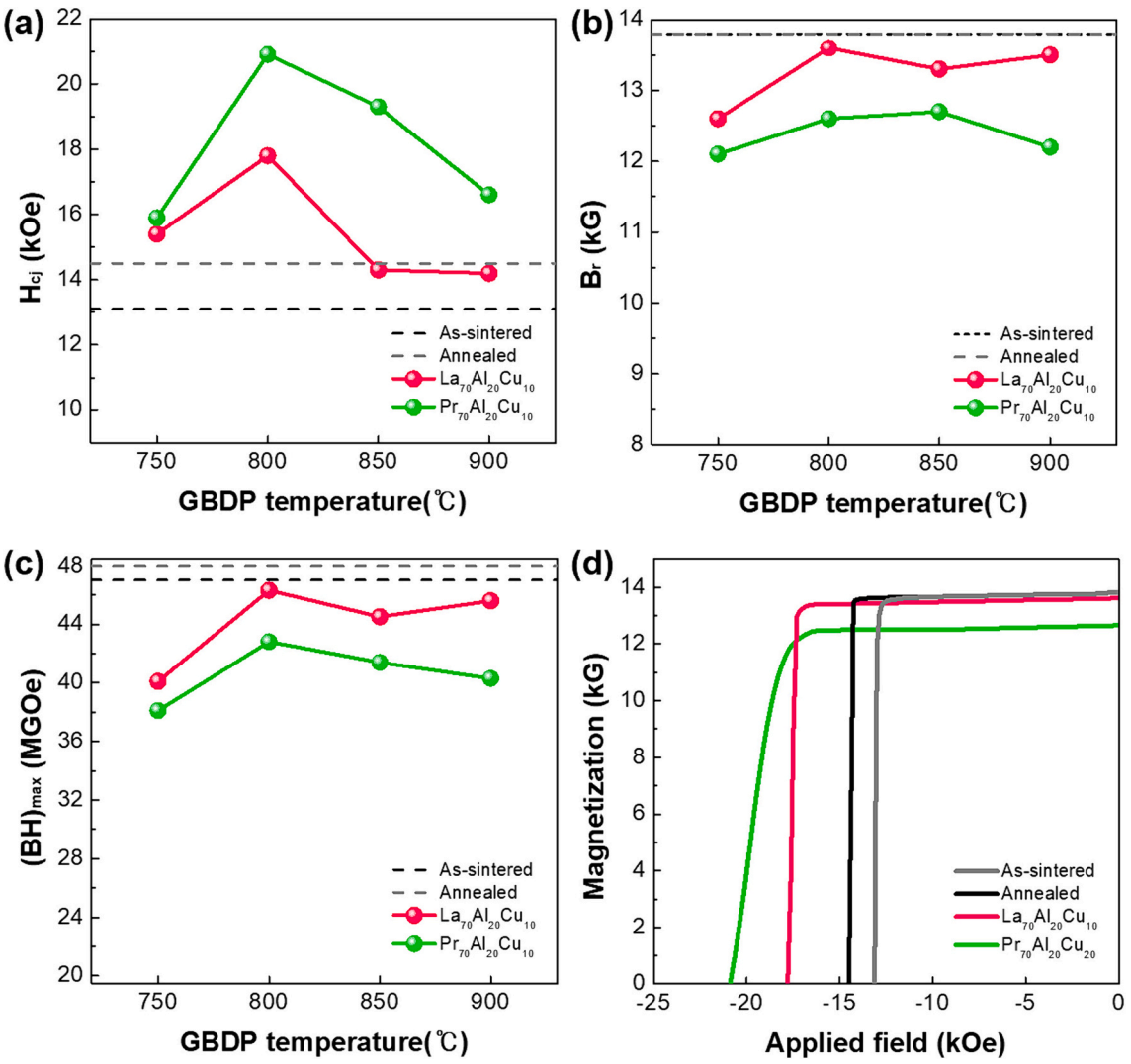

Fig. 1. (a) Intrinsic coercivity (H_{cj}), (b) remanence (B_r), and (c) maximum energy product ($(BH)_{max}$) of Nd–Fe–B sintered magnets GBDP treated with $LRE_{70}Al_{20}Cu_{10}$ (LRE = La and Pr) alloys as a function of diffusion temperatures. (d) Demagnetization curves of the magnets optimally GBDP treated with $LRE_{70}Al_{20}Cu_{10}$. Demagnetization curves of as-sintered base magnet and the reference magnet (heat treated only at 800 °C without GBD) are also shown.

Table 1
Magnetic properties of Nd–Fe–B sintered magnets optimally GBD treated with $La_{70}Al_{20}Cu_{10}$ and $Pr_{70}Al_{20}Cu_{10}$. Magnetic properties of the as-sintered magnet and the annealed magnet (heat treated only at 800 °C and subsequently annealed at 500 °C) are also listed for comparison.

GBDP Materials	GBDP Temperature (°C)	H_{cj} (kOe)	B_r (kG)	$(BH)_{max}$ (MGOe)	SF (%)
As-sintered magnet	–	13.1	13.8	47.0	99
Annealed magnet	800	14.5	13.8	48.0	99
$La_{70}Al_{20}Cu_{10}$	800	17.8	13.6	46.1	98
$Pr_{70}Al_{20}Cu_{10}$	800	20.9	12.6	42.8	86

Thus, the better squareness obtained in the LAC-GBDP magnets implies that such an undesirable grain growth by the CILFM does not occur during LAC-GBDP, *i.e.*, all the diffused La, Al, and Cu in the LAC source do not contribute to shell formation and do not affect the intrinsic magnetic properties of the 2–14-1 main phase, as described above. To elucidate the origin of the improved B_r and squareness of the LAC-GBDP magnets, their microstructures were characterized and compared with those of the PAC-GBDP magnets.

Fig. 2(a) shows the cross-sectional backscattered electron (BSE) images taken from the 50 μm depth from the surface of LAC- and PAC-GBDP magnets, and their schematic illustrations tracing the GBP. In the case of PAC-GBDP sample, the grain size was measured as 7.912 μm, which is much larger than that for the LAC-GBDP (5.632 μm) and annealed base magnets (5.476 μm). In addition, the shape of the GBP in the PAC-GBDP samples appeared curved, whereas those in the LAC-GBDP sample were relatively flat, as shown in Fig. 2 (a). This indicates that the CILFM occurred only in the PAC-GBDP magnet because the grain growth accompanied by GBP bending is a representative microstructural change in magnets where the CILFM occurred during GBDP, as recently reported by Kim *et al* [32]. Because CILFM occurs while leaving the shell behind, shell formation was also observed only in the PAC-GBDP magnet, as shown in Fig. 2(b). Fig. 2(b) shows the electron probe micro-analyzer (EPMA) maps at the depths of 50 μm from the surface of the LAC-, PAC-GBDP magnets. In the PAC-GBDP magnets, the formation of a Pr-rich shell was clearly observed, as shown in the 2nd row of Fig. 2(b). Interestingly, the Al in the PAC source also contributed to shell formation to form a Pr-Al-rich shell. No shell formation was observed for the LAC-GBDP samples, as shown in the 1st row of Fig. 2(b). La, Al, and Cu were distributed along the GBP rather than within the outer region of the 2–14-1 grain.

To confirm the elemental distribution in the GBP region of the

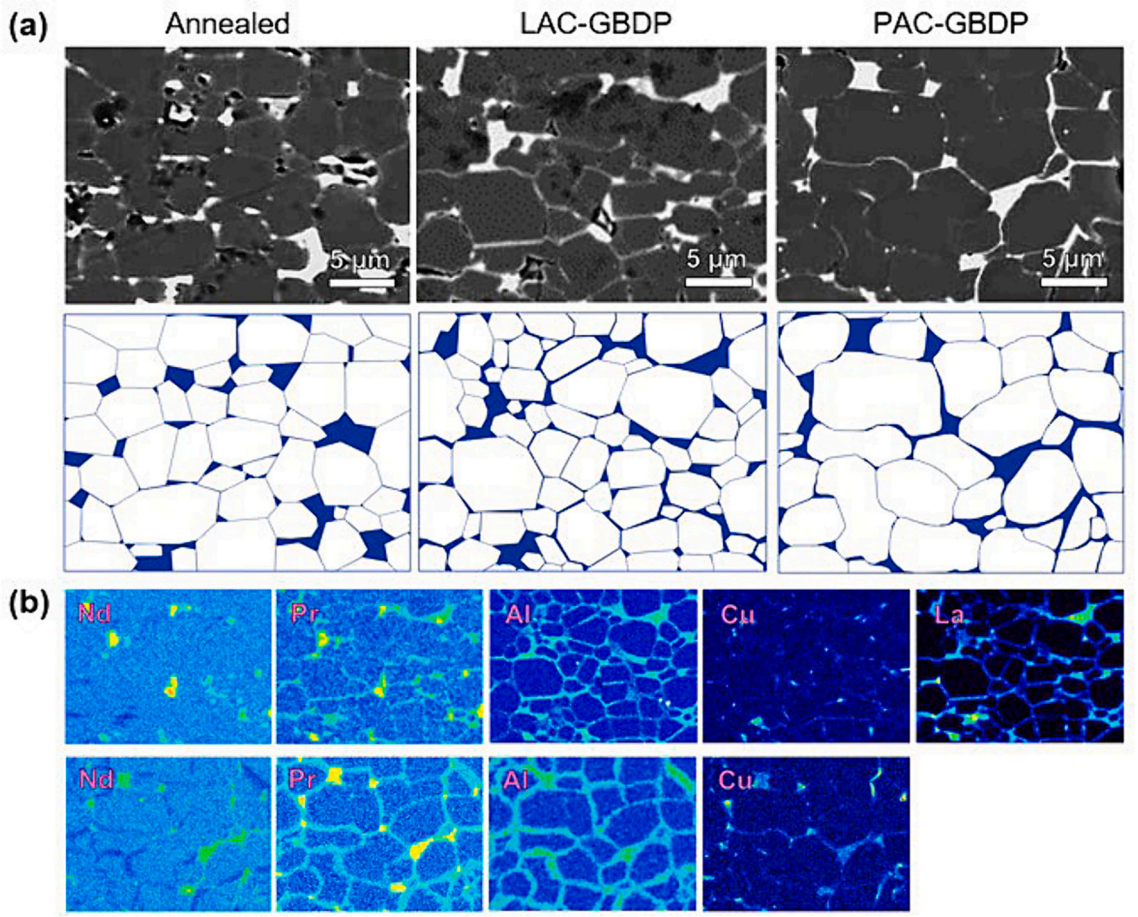

Fig. 2. (a) Cross-sectional BSE-SEM images and schematic illustrations tracing grain boundaries and triple junction phases of as sintered magnet and GBDP magnets observed at a depth of 50 μm from the magnet surface. (b) The EPMA mapping results of Nd, Pr, Fe, Al, Cu and La elements were obtained from the images of LAC-GBDP and PAC-GBDP, respectively, as shown in (a).

samples, high-angle annular dark-field scanning transmission electron microscopy analysis was performed. Fig. 3 shows the HAADF STEM and energy dispersive spectroscopy maps of the GBP formed on the c-plane of the 2–14-1 grain. The line-scan profiles across the GBP of the samples are shown on the right side of the figure. As shown in Fig. 2, La in the LAC-GBDP samples was predominantly concentrated within the GBP, along with Cu. Owing to the larger atomic radius of La (0.195 nm) than that of Nd (0.185 nm), the substitution energy for La in the $Nd_2Fe_{14}B$ phase is positive [39]. In the case of Cu, the solubility of 2–14-1 is almost zero [40]. Thus, La and Cu did not contribute to shell formation and tended to accumulate in the GBP, as shown in Fig. 3(a). In addition, most of the Al in the LAC source segregated at the GBP rather than at the surface of the grains, as shown in Fig. 3(a). Therefore, undesirable grain growth by CILFM does not occur in the magnets during LAC-GBDP, as shown in Fig. 2; thus, the squareness of the magnets is retained after LAC-GBDP, as shown in Fig. 1 [33,34]. This tendency of LAC to segregate into GBP would also be the main contributor to the minimized B_r reduction and H_{cj} enhancement observed in Fig. 1. When the grain boundary-diffused La and Al/Cu were substituted with Nd and Fe to form the LAC-rich shell, the intrinsic M_s of the 2–14-1 phase decreased substantially, as reported by Yu *et al* [41]. However, because the diffusion of LAC into the 2–14-1 is prohibited, the M_s of 2–14-1 is unchanged and only the microstructure of the GBP was affected by the LAC-GBDP, *i.e.,* the thickness of GBP increases from 5 to 10 nm (annealed base magnets, not shown here) to ~130 nm and the concentration of non-ferromagnetic rare-earth (RE), Cu, and Al of GBP increases from 14.3, 1.1, and 1.9 (annealed base magnets, not shown here) to 25.7, 3.2, and 8.7 at.% after the LAC-GBDP. Thereby, the H_{cj} increases by 3.3 kOe and the B_r decreases by only 0.2 kG, as shown in Fig. 1. Unlike the EPMA results shown in Fig. 2, a very thin Al-rich shell (150 nm) appears to form in the LAC-GBDP magnets, as shown in Fig. 3(a). Because the growth rate of the 2–14-1 grains induced by the CILFM is a function of the thickness of the shell formed after GBDP, such a very thin Al-rich shell formation does not induce obvious grain growth after GBDP, as shown in Fig. 2(a). In addition, according to previous investigations, Al dissolution in 2–14-1 increased H_a [42,43]. Therefore, such a thin Al-rich shell at the 2–14-1//GBP interface is also one of the factors responsible for the H_{cj} enhancement after LAC-GBDP. In contrast to the LAC-GBDP magnets, Pr-Al-rich and Al-rich shells were observed on both sides of the GBP in the PAC-GBDP magnet. In the case of the left-side shell, the shell was divided into Pr-Al-rich and Al-rich regions. The Pr and Al contents of the Pr-Al-rich shell were ~ 6.7 and ~ 4.9 at.% respectively, and those of the Al-rich shell are 4.2 at.% and 3.9 at.% respectively. It seems that the shell in the PAC-GBDP magnets was formed by consuming Al preferentially over the Pr during CILFM. For the shell on the right-hand side, only the Pr-Al-rich shell with Pr and Al concentration of 6.5 and 5.9 at.% is formed, as shown in Fig. 3(b). Because of the dissolution of Pr and Al into 2–14-1 to form the Pr-Al-rich shell, H_a of the surface region of the grain is expected to dramatically increased [41–43]. In addition, as shown in the line scan profile in Fig. 3(b), the RE, Al, and Cu concentrations of the GBP in the PAC-GBDP magnets were much higher than those in the LAC-GBDP magnets, indicating that the magnetization of the GBP in the PAC-GBDP magnets was lower than that in the LAC-GBDP magnets. As a result, the H_{cj} achieved by PAC-GBDP is higher than that achieved by LAC-GBDP, as shown in Fig. 1. However, owing to the large amount of Al dissolution into the 2–14-1 and dramatic increase in the

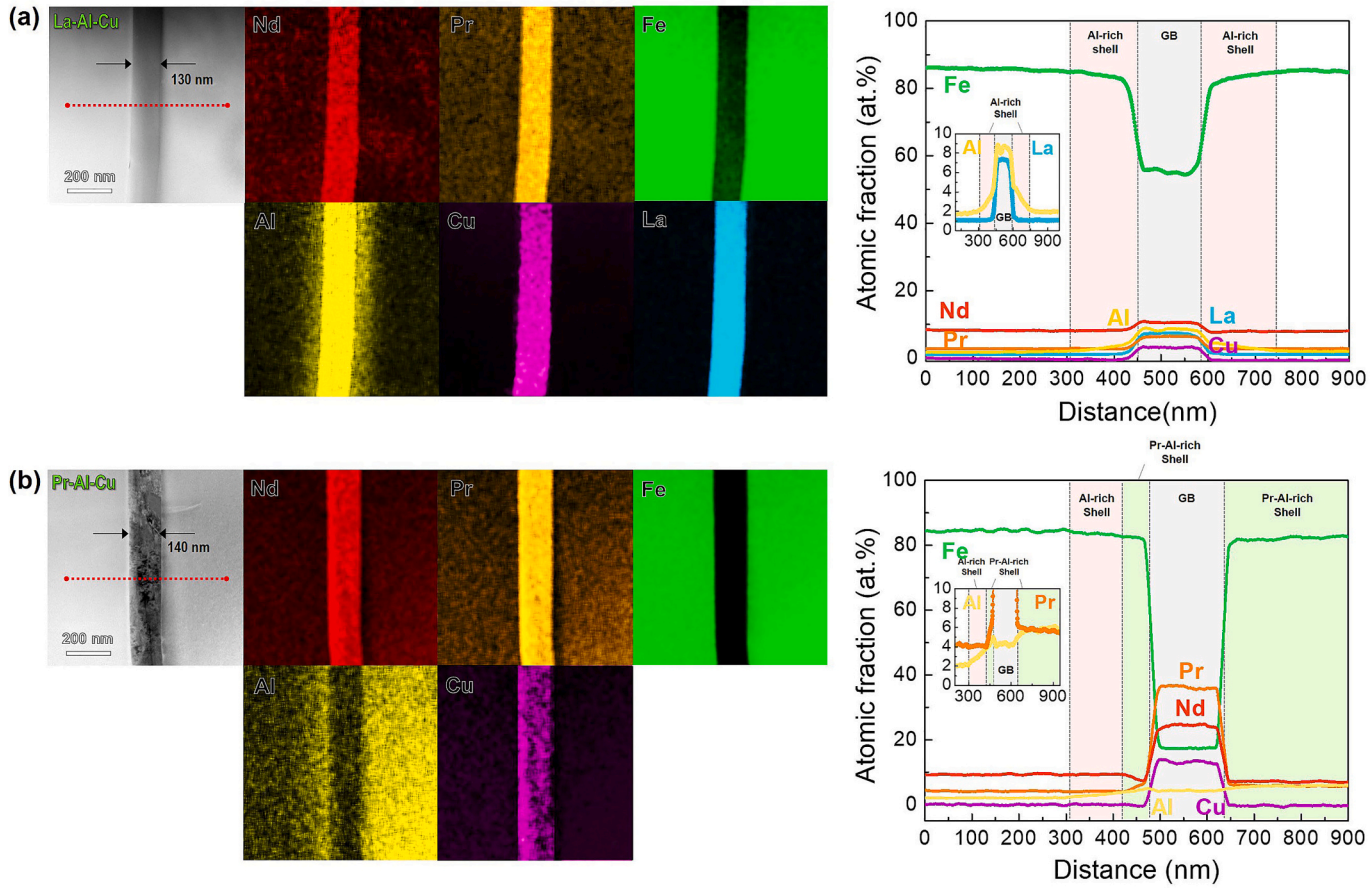

Fig. 3. HAADF-STEM images and EDS elemental near the GBP of (a) LAC-GBDP and (b) PAC-GBDP magnets at a depth of 50 μm from the magnet surface. Line concentration profiles performed across the GBP along the red dotted line marked in the HAADF-STEM images. (For interpretation of the references to colour in this figure legend, the reader is referred to the web version of this article.)

thickness of the nonferromagnetic GBP, as shown in Fig. 2(b) and 3(b), B_r decreased dramatically, as shown in Fig. 1. In addition, as described in Fig. 2, undesirable grain growth by CILFM occurs in the magnets during PAC-GBDP, leading to a deterioration in squareness and $(BH)_{max}$ shown in Fig. 1.

Hereafter, clear microstructural evidence for the CILFM and the contribution of Pr and Al to the CILFM are discussed based on the results from the HAADF-STEM analysis. Fig. 4. shows HAADF-STEM and EDS mapping images of the curved GBP in the PAC-GBDP magnets. The fuzzy dark straight line shown in the HAADF-STEM image is a crack taken place in that occurred during TEM specimen preparation. The EDS elemental mapping images show the asymmetric formation of a Pr-Al-rich shell along the curved GBP. Interestingly, several planar defects were observed near the core–shell interface, as indicated by the black triangles in Fig. 4(a). A high-magnification high-angle annular dark-field (HAADF)-STEM image of the planar defects is shown in Fig. 4(b). Planar defects oriented toward the (001) direction were observed within the 2:14:1 crystal, and a periodic 2:14:1 layer was absent along the core/shell interface. According to a previous investigation on CILFM [32,44–46], the position of such planar defects corresponds to the position of the core//shell interface (position of the initial GBP). This is because an abrupt solidification of the liquid occurs at the core-shell interface when the liquid GBP located at the initial position (*i.e.*, core//shell interface position after GBDP) migrates *via* the CILFM [32,44–46]. To confirm the distributional changes in Pr and Al near these planar defects, line concentration profiles for Nd, Pr, Al, and Fe were obtained across the planar defects (along the white dotted line in the Nd map), as shown in Fig. 4(c). Based on the variation in the concentration of each element, distinct regions corresponding to the Pr-Al-rich shells, Al-rich shells, and defects were identified, as shown in Fig. 4(c). Interestingly, at defect 4, it appears that the Al-rich shell starts to form while consuming only the grain-boundary-diffused Al. The Pr—Al consumption appears to begin at defect 2 to form a Pr-Al-rich shell, as shown in Fig. 4(c). As schematically illustrated in Fig. 4(d), the position of the core//Al-rich shell interface matched that of defects 1 and 4, and the position of the Al-rich shell//Pr-Al-rich shell matched that of defects 2 and 5. This implies that 2-step CILFM occurs in the PAC-GBDP magnets during the shell formation, as shown in Fig. 3(b) and schematically illustrated in Fig. 5. Considering the substitution energy of Al and Pr with Fe and Nd in 2–14-1, Al dissolution into 2–14-1 is much more stable than Pr dissolution into 2–14-1 [47–49]. The phase stability of $Nd_2Fe_{14}B$ is slightly higher than that of $Pr_2Fe_{14}B$ [39]. Therefore, during shell formation by CILFM, the grain boundary diffused Al is consumed first to form the Al-rich shell, and then Pr starts to be involved in shell formation, forming the Pr-Al-rich shell, as shown in Fig. 4 and Fig. 5. Because of the lower stability of $Pr_2Fe_{14}B$ than $Nd_2Fe_{14}B$, the thickness of the Pr-rich shell observed in this study and reported elsewhere is always thinner than that of the Tb-rich shell or Dy-rich shell in the HRE-GBDP magnets because the HRE, contrary to Pr, further stabilizes 2–14-1 when it substitutes Nd in 2–14-1 [35]. According to a micromagnetic simulation [50], the RE concentration of the high-anisotropy RE-rich shell should be controlled to be higher by inhibiting CILFM. Thus, Pr-GBDP, which formed a thin Pr-rich shell, was more advantageous than HRE-GBDP, which formed a thick shell. H_{cj} of Pr-GBDP magnets can be further improved if the Pr concentration of the shell is increased by suppressing its accumulation in GBP, as shown in Fig. 3. Our analysis results imply that the simultaneous utilization of La with Pr as the GBDP source can be a solution for forming thin and high-Pr shells in magnets

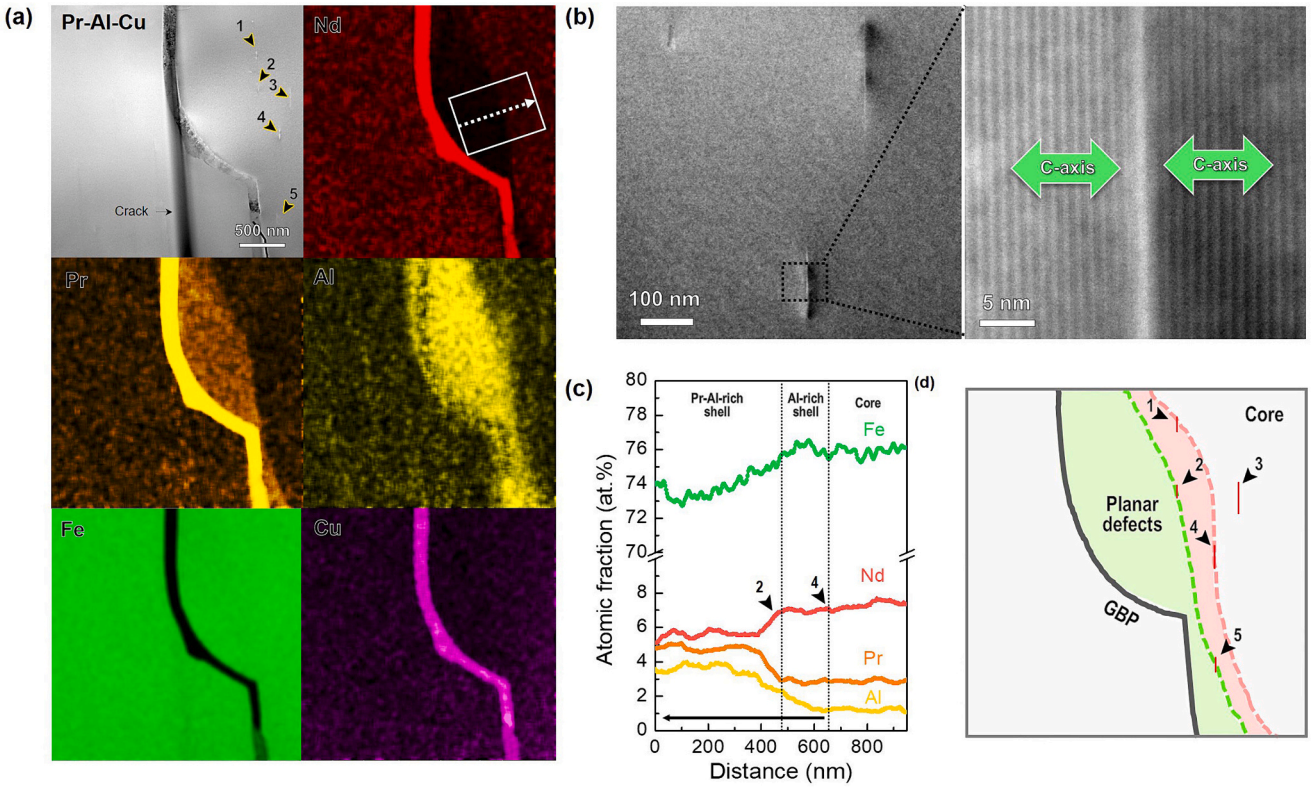

Fig. 4. Structural and compositional analysis of the asymmetric shell observed in the PAC-GBDP magnet: (a) HAADF–STEM image and EDS elemental maps, (b) (left) high-magnification HAADF–STEM image taken from the area marked by the arrow in (a) and (right) high-magnification HAADF–STEM image of a planar defect marked by the black dotted box. (c) line concentration profiles performed across the core–shell interface along the white dotted line marked in the Nd map, (d) schematic of GBP, asymmetric shell and planar defects (red line). The thick dark straight line in the HAADF-STEM image in (a) is a crack taken place in the process of TEM observation. (For interpretation of the references to colour in this figure legend, the reader is referred to the web version of this article.)

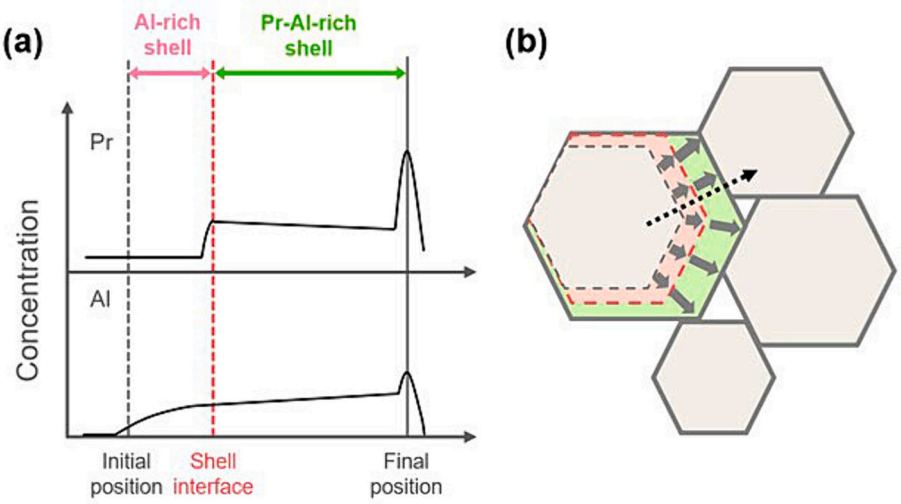

Fig. 5. (a) Concentration variation of solute element Al and Pr across the GBP along the black dotted line marked in (b). (b) Schematic of grain boundary migration and grain growth process of microstructural observation in the magnets GBDP treated with Pr-Al-Cu. Al start to be consumed from initial grain boundary and formed Al-rich shell (pink), and then Pr and Al are consumed together to form the Pr-Al-rich shell (green) with abrupt increase of concentration in Pr. (For interpretation of the references to colour in this figure legend, the reader is referred to the web version of this article.)

because La prefers to dissolve into GBP rather than 2–14-1, as shown in Fig. 3. Due to a high concentration of La in the GBP, the solubility of Pr in the GBP would be decreased, leading to the rejection of the Pr from GBP to the 2–14-1, which in turns increases Pr concentration of the shell. Furthermore, additional grain growth by CILFM due to Al-rich shell formation is expected to be prevented when La is simultaneously utilized with PAC as the GBDP source, as clearly shown in Fig. 3, which leads to improved B_r, squareness, and $(BH)_{max}$ of the PAC-GBDP magnets. In conclusion, alloying La with other low-melting GBDP sources that can form a highly anisotropic RE-rich shell can be a solution for preventing grain growth by CILFM, increasing the RE concentration of the shell and decreasing the cost of the GBDP source.

4. Conclusion

We compared the effect of the grain boundary diffusion process (GBDP) using La-Al-Cu (LAC) and Pr-Al-Cu (PAC) on the microstructure and magnetic properties of Nd-Fe-B sintered magnets. PAC-GBDP enhances the H_{cj} of magnets by forming a high-anisotropy Pr-Al-rich shell. However, the formation of these shells, caused by chemically induced liquid film migration (CILFM), leads to undesirable grain growth, thereby deteriorating the squareness of the magnets. In LAC-GBDP, owing to the low solubility of La in 2–14-1, the grain boundary-diffused LAC source is predominantly dissolved in the RE-rich grain boundary phase (GBP) rather than in the main phase and does not form La-rich or Al-rich shells. Therefore, while LAC-GBDP shows a lower coercivity improvement than PAC-GBDP, it is advantageous for achieving better squareness by suppressing the CILFM induced by shell formation. These results suggest that properly combining La and Pr can form a paramagnetic La-rich GBP and a thin, high-anisotropy Pr-rich shell, which minimizes losses in the remanence, squareness, and $(BH)_{max}$ of the magnets while reducing the GBDP source costs. Our results provide insights into the development of cost-effective LRE-GBDP for fabricating high-performance Nd-Fe-B sintered magnets by utilizing La in combination with other low-melting LRE-GBDP sources.

CRediT authorship contribution statement

Ye Ryeong Jang: Writing – review & editing, Writing – original draft, Methodology, Investigation, Formal analysis, Data curation, Conceptualization. **Tae-Hoon Kim:** Writing – review & editing, Writing – original draft, Visualization, Validation, Formal analysis, Data curation. **Jeongmin Kim:** Writing – review & editing, Writing – original draft, Investigation, Formal analysis. **Hyun-sook Lee:** Writing – original draft, Visualization, Investigation, Conceptualization. **Kyungmi Lee:** Methodology, Investigation, Formal analysis. **Jong Wook Roh:** Visualization, Validation, Funding acquisition, Data curation. **Tae-Suk Jang:** Writing – review & editing, Writing – original draft, Validation, Formal analysis, Data curation, Conceptualization. **Wooyoung Lee:** Writing – review & editing, Validation, Supervision, Project administration, Funding acquisition.

Declaration of competing interest

The authors declare that they have no known competing financial interests or personal relationships that could have appeared to influence the work reported in this paper.

Data availability

Data will be made available on request.

Acknowledgements

This research was supported by the National Research Foundation of Korea (NRF) and a Commercialization Promotion Agency for R&D Outcomes (COMPA) grant funded by the Korean government (MSIT) (RS-2023-00238493), Technology Innovation Program (2001362, Center for Super Critical Material Industrial Technology) funded by the Ministry of Trade, Industry & Energy (MOTIE, Korea); and Basic Science Research Program through the National Research Foundation of Korea (NRF) funded by the Ministry of Education (NRF2019R1A6A1A11055660).

References

[1] R.H.J. Fastenau, E.J. vanLoenen, Applications of rare earth permanent magnets, J. Magn. Magn. Mater. 157 (1996) 1–6.
[2] Y. Luo, Development of NdFeB magnet industry in new century, J. Iron Steel Res. Int. 13 (2006) 1–11.
[3] D. Brown, B.M. Ma, Z.M. Chen, Developments in the processing and properties of NdFeb-type permanent magnets, J. Magn. Magn. Mater. 248 (2002) 432–440.
[4] M.D. Calin, E. Helerea, Temperature Influence on Magnetic Characteristics of NdFeB Permanent Magnets, Int Symp Adv Top, 2011.
[5] S. Hirosawa, Y. Matsuura, H. Yamamoto, S. Fujimura, M. Sagawa, H. Yamauchi, Magnetization and magnetic-anisotropy of R2fe14b measured on single-crystals, J. Appl. Phys. 59 (1986) 873–879.
[6] K. Hono, H. Sepehri-Amin, Prospect for HRE-free high coercivity Nd-Fe-B permanent magnets, Scr. Mater. 151 (2018) 6–13.
[7] K. Binnemans, P.T. Jones, B. Blanpain, T. Van Gerven, Y.X. Yang, A. Walton, M. Buchert, Recycling of rare earths: a critical review, J. Clean. Prod. 51 (2013) 1–22.
[8] K. Hirota, H. Nakamura, T. Minowa, M. Honshima, Coercivity enhancement by the grain boundary diffusion process to Nd-Fe-B sintered magnets, IEEE Trans. Magn. 42 (2006) 2909–2911.
[9] F. Chen, L. Zhang, Y. Jin, Experimental and computational analysis of the two-step demagnetization behavior of the surface grains of sintered Nd-Fe-B magnets, J. Appl. Phys. 124 (2018) 053902.
[10] K. Hono, H. Sepehri-Amin, Strategy for high-coercivity Nd–Fe–B magnets, Scr. Mater. 67 (2012) 530–535.
[11] G. Hrkac, T.G. Woodcock, C. Freeman, A. Goncharov, J. Dean, T. Schrefl, O. Gutfleisch, The role of local anisotropy profiles at grain boundaries on the coercivity of Nd 2 Fe 14 B magnets, Appl. Phys. Lett. 97 (2010) 232511.
[12] H. Sepehri-Amin, D. Prabhu, M. Hayashi, T. Ohkubo, K. Hioki, A. Hattori, K. Hono, Coercivity enhancement of rapidly solidified Nd-Fe-B magnet powders, Scr. Mater. 68 (2013) 167–170.
[13] T. Akiya, J. Liu, H. Sepehri-Amin, T. Ohkubo, K. Hioki, A. Hattori, K. Hono, High-coercivity hot-deformed Nd-Fe-B permanent magnets processed by Nd-cu eutectic diffusion under expansion constraint, Scr. Mater. 81 (2014) 48–51.
[14] H. Sepehri-Amin, T. Ohkubo, S. Nagashima, M. Yano, T. Shoji, A. Kato, T. Schrefl, K. Hono, High-coercivity ultrafine-grained anisotropic Nd-Fe-B magnets processed by hot deformation and the Nd-cu grain boundary diffusion process, Acta Mater. 61 (2013) 6622–6634.
[15] S. Lee, J. Kwon, H.R. Cha, K.M. Kim, H.W. Kwon, J. Lee, D. Lee, Enhancement of Coercivity in sintered Nd-Fe-B magnets by grain-boundary diffusion of electrodeposited cu-Nd alloys, Met. Mater. Int. 22 (2016) 340–344.
[16] T. Akiya, J. Liu, H. Sepehri-Amin, T. Ohkubo, K. Hioki, A. Hattori, K. Hono, Low temperature diffusion process using rare earth-cu eutectic alloys for hot-deformed Nd-Fe-B bulk magnets, J. Appl. Phys. 115 (2014).
[17] M. Lv, T. Kong, W.H. Zhang, M.Y. Zhu, H.M. Jin, W.X. Li, Y. Li, Progress on modification of microstructures and magnetic properties of Nd-Fe-B magnets by the grain boundary diffusion engineering, J. Magn. Magn. Mater. 517 (2021).
[18] X. Tang, H. Sepehri-Amin, T. Ohkubo, K. Hono, Suppression of non-oriented grains in Nd-Fe-B hot-deformed magnets by Nb doping, Scr. Mater. 147 (2018) 108–113.
[19] H. Zeng, Z. Liu, J. Zhang, X. Liao, H. Yu, Towards the diffusion source cost reduction for NdFeB grain boundary diffusion process, J. Mater. Sci. Technol. 36 (2020) 50–54.
[20] H. Zeng, H. Yu, Q. Zhou, J. Zhang, X. Liao, Z. Liu, Clarifying the effects of La and Ce in the grain boundary diffusion sources on sintered NdFeB magnets, Mater. Res. Express 6 (2019) 106105.
[21] H. Zeng, Q. Wang, J. Zhang, X. Liao, X. Zhong, H. Yu, Z. Liu, Grain boundary diffusion treatment of sintered NdFeB magnets by low cost La-Al-cu alloys with various Al/cu ratios, J. Magn. Magn. Mater. 490 (2019) 165498.
[22] T. Akiya, J. Liu, H. Sepehri-Amin, T. Ohkubo, K. Hioki, A. Hattori, K. Hono, High-coercivity hot-deformed Nd–Fe–B permanent magnets processed by Nd–cu eutectic diffusion under expansion constraint, Scr. Mater. 81 (2014) 48–51.
[23] S. Lee, J. Kwon, H.-R. Cha, K.M. Kim, H.-W. Kwon, J. Lee, D. Lee, Enhancement of coercivity in sintered Nd-Fe-B magnets by grain-boundary diffusion of electrodeposited cu-Nd alloys, Met. Mater. Int. 22 (2016) 340–344.
[24] F. Chen, T. Zhang, J. Wang, L. Zhang, G. Zhou, Coercivity enhancement of a Nd-Fe-B sintered magnet by diffusion of Nd70Cu30 alloy under pressure, Scr. Mater. 107 (2015) 38–41.
[25] M.H. Tang, X.Q. Bao, K.C. Lu, L. Sun, J.H. Li, X.X. Gao, Boundary structure modification and magnetic properties enhancement of Nd-Fe-B sintered magnets by diffusing (PrDy)-cu alloy, Scr. Mater. 117 (2016) 60–63.
[26] H. Zeng, Z. Liu, W. Li, J. Zhang, L. Zhao, X. Zhong, H. Yu, B. Guo, Significantly enhancing the coercivity of NdFeB magnets by ternary Pr-Al-cu alloys diffusion and understanding the elements diffusion behavior, J. Magn. Magn. Mater. 471 (2019) 97–104.
[27] Y. Huang, Y. Yao, F.Y. Wang, H. Li, Z. Wu, Q. Feng, W. Li, J. Luo, Z. Pang, C. Zhong, Y. Hou, Improving intergranular phase and enhanced coercivity: a grain boundary diffusion of non- heavy rare earth PrNdAl alloy in sintered Nd-Fe-B magnets, J. Mater. Res. Technol. 21 (2022) 4320–4329.
[28] H. Sepehri-Amin, L.H. Liu, T. Ohkubo, M. Yano, T. Shoji, A. Kato, T. Schrefl, K. Hono, Microstructure and temperature dependent of coercivity of hot-deformed Nd-Fe-B magnets diffusion processed with Pr-cu alloy, Acta Mater. 99 (2015) 297–306.
[29] M. Yan, W. Chen, J.Y. Jin, Y.S. Liu, H.S. Chen, S.P. Ringer, J.J. Xu, Y.L. Hou, M. Yue, X.L. Liu, Merits of Pr80Ga20 grain boundary diffusion process towards high coercivity-remanence synergy of Nd-La-Ce-Fe-B sintered magnet, Acta Mater. 231 (2022).
[30] S.N. Fan, M.X. Jin, G.F. Ding, X.D. Fan, S. Guo, B. Zheng, R.J. Chen, A.R. Yan, B. Meng, Evaluation of core-shell structure and grain boundary structure in multi-main-phase Nd-Y-Fe-B sintered magnet by grain boundary modification, J. Alloys Compd. 932 (2023).

[31] X.T. Yang, S. Cao, M.P. Kou, Z. Jia, G.F. Ding, W.Z. Yin, R.J. Chen, A.R. Yan, Microstructure and coercivity modification of HDDR (Pr, Nd, Ce)-Fe-B magnetic powders by grain boundary diffusion with Pr-Fe-Al-Ga, Mater. Lett. 341 (2023).
[32] T.H. Kim, T.T. Sasaki, T. Koyama, Y. Fujikawa, M. Miwa, Y. Enokido, T. Ohkubo, K. Hono, Formation mechanism of Tb-rich shell in grain boundary diffusion processed Nd-Fe-B sintered magnets, Scr. Mater. 178 (2020) 433–437.
[33] E.A. Périgo, H. Takiishi, C.C. Motta, R.N. Faria, Microstructure and squareness factor:: A quantitative correlation in (Nd, Pr)FeB sintered magnets, J. Appl. Phys., 102 (2007).
[34] X. Tang, J. Li, H. Sepehri-Amin, T. Ohkubo, K. Hioki, A. Hattori, K. Hono, Improved coercivity and squareness in bulk hot-deformed Nd-Fe-B magnets by two-step eutectic grain boundary diffusion process, Acta Mater. 203 (2021).
[35] L.Z. Zhao, J.Y. He, W. Li, X.L. Liu, J. Zhang, L. Wen, Z.H. Zhang, J.W. Hu, J. S. Zhang, X.F. Liao, K. Xu, W.B. Fan, W.Y. Song, H.Y. Yu, X.C. Zhong, Z.W. Liu, X. F. Zhang, Understanding the role of element grain boundary diffusion mechanism in Nd-Fe-B magnets, Adv. Funct. Mater. 32 (2022).
[36] M.P. Kou, S. Cao, T.F. Wu, Y.H. Xie, Z. Jia, H.B. Luo, X.D. Fan, G.F. Ding, B. Zheng, R.J. Chen, S. Guo, A.R. Yan, Coercivity and thermal stability enhancement of Nd-Fe-B magnet by grain boundary diffusing Tb-Y-La-cu alloys, J. Alloys Compd. 945 (2023).
[37] Y.J. Wong, H.W. Chang, Y.I. Lee, W.C. Chang, C.H. Chiu, C.C. Mo, Comparison on the coercivity enhancement of sintered NdFeB magnets by grain boundary diffusion with low-melting (Tb, R)-cu alloys (R= none, Y, La, and Ce), AIP Adv. 9 (2019).
[38] J.F. Herbst, R2fe14b materials - intrinsic-properties and technological aspects, Rev. Mod. Phys. 63 (1991) 819–898.
[39] X.B. Liu, Z. Altounian, M.D. Huang, Q.M. Zhang, J.P. Liu, The partitioning of La and Y in Nd-Fe-B magnets: a first-principles study, J. Alloys Compd. 549 (2013) 366–369.
[40] O.M. Ragg, I.R. Harris, A study of the effects of heat-treatment on the microstructures and magnetic-properties of cu-added Nd-Fe-B type sintered magnets, J. Alloys Compd. 209 (1994) 125–133.
[41] X.Q. Yu, M. Yue, W.Q. Liu, Z. Li, M.G. Zhu, S.Z. Dong, Structure and intrinsic magnetic properties of MM2Fe14B (MM=La, Ce, Pr, Nd) alloys, J. Rare Earths 34 (2016) 614–617.
[42] S. Hirosawa, Y. Yamaguchi, K. Tokuhara, H. Yamamoto, S. Fujimura, M. Sagawa, Magnetic-properties of Nd2(Fe1-Xalx)14b, Nd2(Fe1-Xcrx)14b, Nd2(Fe1-Xmnx)14b and Nd2(Fe1-Xcox)14b measured on single-crystals, IEEE Trans. Magn. 23 (1987) 2120–2123.
[43] J. Strzeszewski, G.C. Hadjipanayis, A.S. Kim, The effect of Al substitution on the Coercivity of Nd-Fe-B magnets, J. Appl. Phys. 64 (1988) 5568–5570.
[44] H.K. Kang, S. Hackney, D.N. Yoon, Migration of liquid-film and grain-boundary in Mo-Ni induced by W-diffusion, Acta Metall. Mater. 36 (1988) 695–699.
[45] Y.J. Baik, K.Y. Eun, Chemically-induced migration of liquid-films and grain-boundaries in tin-Ni-(tic) alloy, J. Am. Ceram. Soc. 74 (1991) 1397–1400.
[46] Y.J. Baik, D.N. Yoon, Chemically-induced migration of liquid-films and grain-boundaries in Mo-Ni-(Fe) alloy, Acta Metall. 34 (1986) 2039–2044.
[47] B. Grieb, K.G. Knoch, E.T. Henig, G. Petzow, Influence of Al-based additions on Coercivity and microstructure in Fe-Nd-B magnets, J. Magn. Magn. Mater. 80 (1989) 75–79.
[48] K.G. Knoch, B. Grieb, E.T. Henig, H. Kronmuller, G. Petzow, Upgraded Nd-Fe-B-Al, Nd-Fe-B-Ga magnets - wettability and microstructure, IEEE Trans. Magn. 26 (1990) 1951–1953.
[49] A. Takeuchi, A. Inoue, Classification of bulk metallic glasses by atomic size difference, heat of mixing and period of constituent elements and its application to characterization of the main alloying element, Mater. Trans. 46 (2005) 2817–2829.
[50] T. Oikawa, H. Yokota, T. Ohkubo, K. Hono, Large-scale micromagnetic simulation of Nd-Fe-B sintered magnets with Dy-rich shell structures, AIP Adv. 6 (2016).